Chinese Journal of
POLYMER SCIENCE

RESEARCH ARTICLE

https://doi.org/10.1007/s10118-026-3700-z
Chinese J. Polym. Sci.

Squaramide-directed Cooperative One-dimensional Assembly in Telechelic Polydimethylsiloxane for Hierarchical Network Formation

Yu-Hong Zhang[a,†], Jian-Fei Ma[a,†], Hao-Bo Wei[a], Jie Wang[b], and Feng Wang[a*]

[a] *Department of Polymer Science and Engineering, University of Science and Technology of China, Hefei 230026, China*
[b] *School of Chemistry and Pharmaceutical Engineering, Jilin University of Chemical Technology, Jilin 132022, China*

Electronic Supplementary Information

Abstract Polymer crosslinked networks often face a fundamental trade-off between the mechanical robustness of covalent systems and the dynamic reversibility of supramolecular assemblies. Inspired by the hierarchical organization of biological extracellular matrix, where fibrous structures are reinforced by covalent crosslinking, we report a squaramide-directed cooperative assembly strategy that integrates one-dimensional (1D) supramolecular nanofiber formation with covalent macromolecular architecture to construct hierarchical polymer networks. Telechelic macromolecules were designed by tethering orthogonally arranged squaramide–amide hydrogen-bonding motifs to polydimethylsiloxane (PDMS) spacers. In the model system, these motifs undergo cooperative nucleation-elongation assembly into long-range nanofibers, while comparison with a urea analogue reveals enhanced intermolecular binding and assembly stability arising from the squaramide motif. Covalent integration of the assembling units transforms discrete nanofibers into microphase-separated networks with increased thermal stability and storage modulus. This work establishes a molecular design principle linking cooperative self-assembly with hierarchical polymer network formation and macroscopic mechanical performance.

Keywords Cooperative assembly; Squaramide; Telechelic polymers; Hydrogen bonding; Hierarchical polymer networks

Citation: Zhang, Y. H.; Ma, J. F.; Wei, H. B.; Wang, J.; Wang, F. Squaramide-directed cooperative one-dimensional assembly in telechelic polydimethylsiloxane for hierarchical network formation. *Chinese J. Polym. Sci*. https://doi.org/10.1007/s10118-026-3700-z

INTRODUCTION

Polymer-crosslinked networks represent a central class of materials whose macroscopic mechanical properties are governed by molecular connectivity and network architecture.[1–4] These systems are generally categorized as covalent or supramolecular networks (Scheme 1a). Covalent networks provide permanent crosslinks that impart high modulus and structural stability but inherently lack dynamic adaptability.[5–7] In contrast, supramolecular polymer networks rely on reversible non-covalent interactions, enabling responsiveness and self-healing behavior,[8,9] yet often suffer from insufficient mechanical robustness due to the limited strength and lifetime of these interactions.[10–12] Reconciling the mechanical integrity with dynamic reversibility within a single polymer architecture remains a fundamental challenge in network design.

Hierarchically organized biological networks provide a conceptual framework for addressing this dilemma.[13–17] In systems such as extracellular matrix (ECM) networks (Scheme 1b), cooperative noncovalent interactions drive the formation of one-dimensional (1D) fibrous structures, which are subsequently reinforced through covalent crosslinking at higher hierarchical levels.[18–22] Mechanical resilience emerges from the integration of directional supramolecular organization and covalent network stabilization across multiple length scales.[23–26]

Translating this hierarchical principle into synthetic polymers requires engineering noncovalent interactions that are sufficiently strong to generate long-range ordered 1D nanofibers capable of serving as network precursors.[27–29] A viable strategy is to exploit multivalency and directionality to promote cooperative nucleation-elongation assembly.[30–33] Hydrogen-bonding motifs such as benzene-1,3,5-tricarboxamide and bisurea systems exemplify this concept by forming 1D nanofibers through well-defined hydrogen-bond arrays.[34,35] However, their symmetric and predictable binding geometries often limit architectural diversity.[36] Heterogeneous hydrogen-bonding motifs offer increased structural complexity, yet heterogeneity often disrupts cooperativity because different hydrogen-bonding units may exhibit mismatched binding strengths or competing recognition modes, thereby impeding long-range fiber growth and hierarchical organization.[37,38] Designing heterogeneous hydrogen-bonding systems that maintain both interaction hierarchy and cooperative assembly remains an important challenge.

* Corresponding author, E-mail: drfwang@ustc.edu.cn
† These authors contributed equally to this work.
Special Topic: Chirality in Polymers
Received April 10, 2026; Accepted May 4, 2026; Published online July 6, 2026

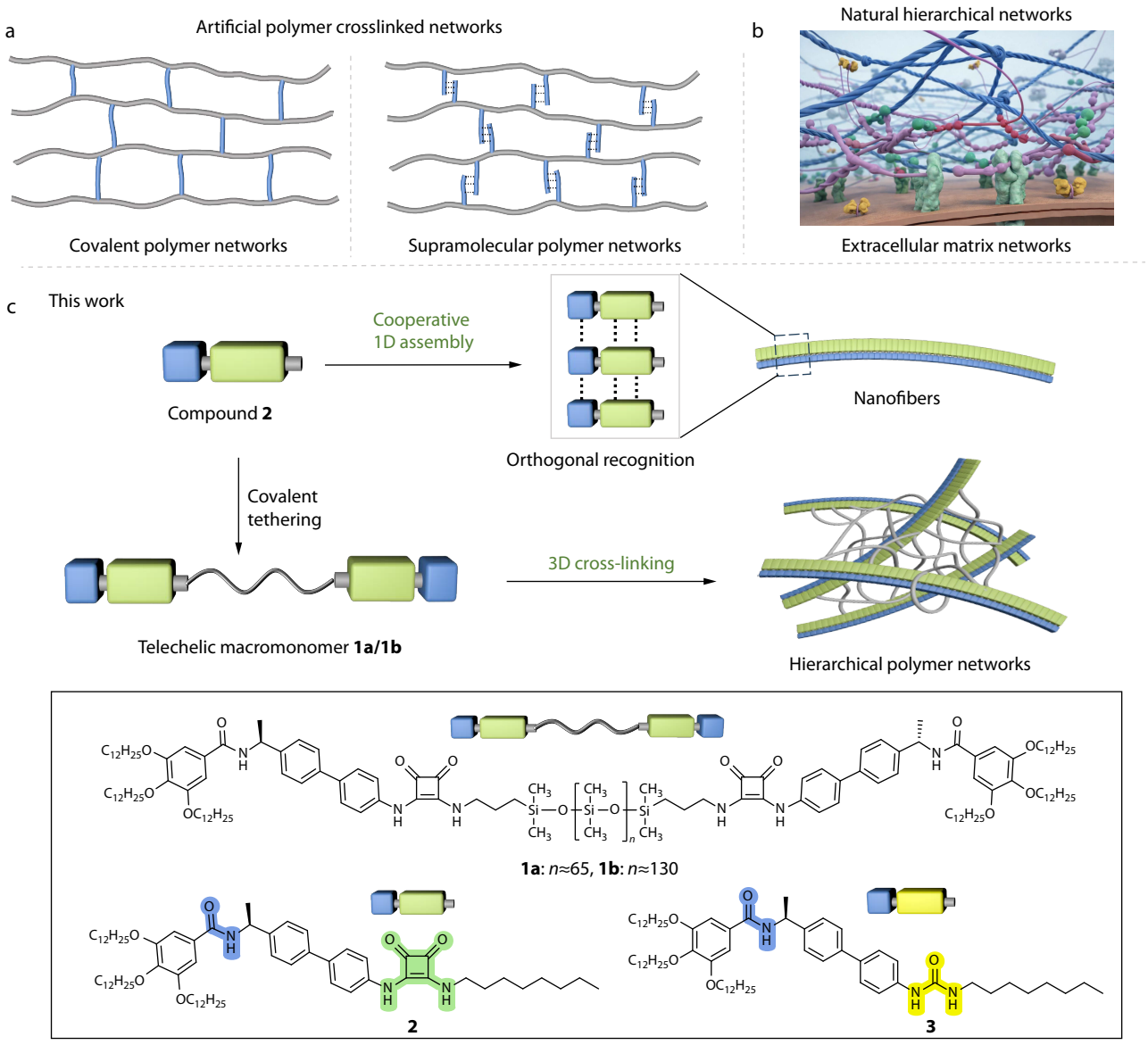

Scheme 1 (a) Schematic illustration of artificial polymer crosslinked networks, including covalent polymer networks and supramolecular polymer networks; (b) Natural hierarchical networks exemplified by the extracellular matrix. (Reproduced from Ref. [19]; licensed under CC BY 3.0.) (c) Schematic illustration of this work. Compound **2** undergoes cooperative 1D assembly through orthogonal hydrogen-bond recognition to form supramolecular nanofibers. Covalent tethering of the assembling motifs to PDMS spacers yields telechelic macromonomers **1a** or **1b**, which further form three-dimensional crosslinked hierarchical polymer networks. The chemical structures of the designed and the control compounds are shown in the frame.

In this study, we address this issue using a squaramide-directed cooperative 1D assembly strategy. We designed telechelic macromolecules **1a/1b** and corresponding model compound **2** incorporating orthogonally arranged squaramide and amide recognition units (Scheme 1c). In the model system, these motifs engage in directional hydrogen bonding, which promotes cooperative nucleation-elongation assembly into long-range 1D nanofibers. Comparative analysis with structurally analogous urea derivative **3** (Scheme 1c) revealed the critical role of squaramide in enhancing intermolecular binding and assembly stability. Building on this, the squaramide–amide motif was covalently tethered to the termini of polydimethylsiloxane (PDMS) to generate telechelic macromolecules **1a/1b**. The PDMS spacer provided covalent connectivity and segmental mobility, enabling the integration of discrete nanofibers into covalently interconnected microphase-separated networks. By varying the ratio between the assembled segments and PDMS spacers, we established a direct correlation between the hydrogen-bond density, supramolecular organization, and macroscopic mechanical properties.

EXPERIMENTAL

Materials and Methods

Diethyl squarate, 4-aminophenylboronic acid pinacol ester,

tetrakis(triphenylphosphine) palladium(0) [$Pd(PPh_3)_4$], octylamine, octyl isocyanate, and aminopropyl-terminated PDMS were of reagent grade and used as received. All other reagents and solvents were used as received. Compounds **9**, **10** (Scheme S1 in the electronic supplementary information, ESI) and **12** were synthesized according to previously reported methods.[39,40]

All moisture- or oxygen-sensitive reactions were performed using the Schlenk technique under a nitrogen atmosphere. ^{1}H- and ^{13}C-NMR spectra were recorded on a Bruker DMX-400 instrument (400 MHz for ^{1}H and 101 MHz for ^{13}C). MALDI-TOF measurements were recorded on a Bruker Autoflex Speed spectrometer with DCTB as the matrix. UV-Vis spectra were recorded on a UV-1800 Shimadzu spectrometer. Circular dichroism (CD) measurements were performed on a Jasco J-1500 circular dichroism spectrometer equipped with a PFD-425S/15 Peltier-type temperature controller. AFM measurements (tapping mode) were performed using a Bruker Dimension Icon with ScanAsyst system in air with silica cantilevers (RFESPA-75, Ohm-cm Antimony (n) doped Si), a resonance frequency of about 75 kHz, and a spring constant of about 3 $N{\cdot}m^{-1}$. The obtained images were analyzed using Pico Image processing software. Differential scanning calorimetry (DSC) was carried out using a TA DSCQ2000 (USA) at a heating rate of 10 °C·min^{-1} from 20 °C to 300 °C. Frequency-dependent rheological tests were performed using a TA DHR 20 rheometer.

DFT Theoretical Calculations

All the DFT calculations were performed using the Gaussian 16 C.01 software package. The Sx Hybrid functional B3LYP with dispersion correction in revision three (DFT-D3) was used. During structure optimization, all atoms were described using the 6-31G(d) basis set. Frequency calculations demonstrated that all optimized geometries were absent from the imaginary frequencies, confirming that these structures are potential energy minima.[41]

Mass-balance Model for 1D Nanofiber Assembly

Compound **2** undergoes a cooperative assembly mechanism upon cooling or heating. The thermodynamic parameters of the 1D nanofiber assembly of **2** were acquired by fitting the melting curve spectroscopy data with the one-component model for the 1D nanofiber assembly. The fitted parameters for the supramolecular fibers of compound **2** are the enthalpy of elongation ΔH_e, the enthalpy of nucleation ΔH_n and the entropy term ΔS_e. The entropy term is the same for both nucleation and elongation. These parameters are related to the equilibrium constants of the elongation phase as follows:

$$K_e = \exp(-\Delta G_e/RT) \quad (1)$$

$$\text{with } \Delta G_e = \Delta H_e - T\Delta S_e \quad (2)$$

and of the nucleation phase (with nucleation penalty NP_e) by

$$K_n = \sigma_e \times K_e \quad (3)$$

$$\text{with } \sigma_e = \exp(-NP_e/RT) \quad (4)$$

$$NP_e = \Delta H_e - \Delta H_n \quad (5)$$

The model was fitted to the experimentally obtained melting curves of samples with varying monomer concentrations. The melting curves were normalized by the total monomer concentration to weigh all the samples equally during the fitting procedure. The fitting parameters used were the entropy and enthalpy of elongation, and the nucleation penalty.

The entropy was sampled between −0.050 and −0.800 $kJ{\cdot}mol^{-1}{\cdot}K^{-1}$, and the Gibbs free energy was sampled between −20 and −220 $kJ{\cdot}mol^{-1}$ to determine the enthalpy and the nucleation penalty between −5 and −35 $kJ{\cdot}mol^{-1}$. The lhsdesign function in MATLAB was used to create 500 initial parameter sets using Latin hypercube sampling. Each of these initial parameter sets was optimized to minimize the sum of squares of the cost vector by using the Levenberg-Marquardt algorithm. MATLAB function lsqnonlin was used to minimize the cost vector and select the lowest norm of the residual sum of squares.

Synthesis of Compound 2

The synthetic route is shown in Fig. S2 (in ESI). A mixture of compound **7** (200 mg, 0.20 mmol), octylamine (31 mg, 0.24 mmol), and trimethylamine (0.5mL) was dissolved in chloroform (30 mL) and stirred at 70 °C for 12 h. After evaporating the solvent under reduced pressure, the residue was purified by flash column chromatography (dichloromethane/acetonitrile, 10/1 *V/V* as the eluent) to afford compound **2** as a pale yellow solid (110 mg, 51% yield). ^{1}H-NMR (400 MHz, 10% TFA in $CDCl_3$, Fig. S25 in ESI, δ, ppm): 7.68 (d, *J*=8.0 Hz, 2H), 7.59 (d, *J*=8.0 Hz, 2H), 7.46 (d, *J*=7.9 Hz, 2H), 7.24 (s, 2H), 6.92 (s, 2H), 5.33 (q, *J*=6.9 Hz, 1H), 4.11 (t, *J*=6.9 Hz, 2H), 4.01 (t, *J*=6.5 Hz, 4H), 3.78 (s, 2H), 1.77 (m, 6H), 1.68 (d, *J*=6.7 Hz, 3H), 1.43 (q, *J*=7.5 Hz, 6H), 1.40–1.19 (m, 60H), 0.87 (q, *J*=6.8 Hz, 12H), 0.14 – 0.07 (m, 6H). ^{13}C-NMR (101 MHz, 10% TFA in $CDCl_3$, Fig. S26 in ESI, δ, ppm): 159.95, 159.54, 159.12, 158.71, 153.28, 141.23, 139.12, 128.24, 127.25, 126.81, 116.23, 113.39, 110.55, 105.90, 77.36, 74.32, 69.71, 32.08, 32.06, 31.84, 30.89, 30.19, 29.88, 29.84, 29.80, 29.76, 29.67, 29.53, 29.51, 29.37, 29.24, 29.18, 26.42, 26.16, 26.07, 22.83, 22.71, 21.78, 14.24, 14.14. MALDI-TOF ($[M+H]^+$): *m/z* 1076.031 (Fig. S27 in ESI).

Synthesis of Compound 3

The synthetic route is shown in Fig. S3 (in ESI). Compound **8** (348 mg, 0.4 mmol) and triethylamine (0.5 mL) were dissolved in dichloromethane (30 mL) at 0 °C. The mixture was then purged with nitrogen for 10 min. Octyl isocyanate (75 mg, 0.48 mmol) dissolved in dichloromethane (5 mL) was added dropwise to this solution. The reaction mixture was stirred at 0 °C for 2 h, warmed to room temperature, and stirred for an additional 12 h. After evaporating the solvent under reduced pressure, the residue was purified by flash column chromatography (dichloromethane as the eluent) to afford compound **3** as a white solid (262 mg, 64% yield). ^{1}H-NMR (400 MHz, $CDCl_3$, Fig. S28 in ESI, δ, ppm): 7.46 (d, *J*=7.9 Hz, 2H), 7.40 (t, *J*=7.1 Hz, 4H), 7.24 (s, 1H), 6.98 (s, 2H), 6.87 (s, 1H), 6.42 (d, *J*=7.8 Hz, 1H), 5.32 (t, *J*=7.2 Hz, 1H), 3.98 (q, *J*=6.0 Hz, 6H), 3.28–3.18 (m, 2H), 1.76 (m, 11H), 1.46 (s, 13H), 1.26 (d, *J*=8.6 Hz, 70H), 0.91–0.82 (m, 14H). ^{13}C-NMR (101 MHz, $CDCl_3$, Fig. S29 in ESI, δ, ppm): 167.16, 156.14, 153.29, 141.76, 141.41, 139.85, 138.87, 134.76, 129.33, 127.52, 127.02, 126.57, 120.07, 105.87, 77.36, 73.69, 69.53, 49.41, 40.87, 40.38, 32.07, 31.96, 31.94, 30.46, 30.40, 30.31, 29.90, 29.85, 29.80, 29.74, 29.58, 29.54, 29.52, 29.50, 29.45, 29.42, 29.38, 27.12, 27.04, 26.24, 22.84, 22.79, 22.25, 14.27, 14.24. MALDI-TOF ($[M + H]^+$): *m/z* 1024.112 (Fig. S30 in ESI).

Synthesis of Compounds 1a/1b

The synthetic route is shown in Fig. S4 (in ESI). A mixture of compound **7** (210 mg, 0.21 mmol), PDMS ($M_n \approx 5$ kg/mol, 500 mg, 0.10 mmol), and triethylamine (0.5 mL) in toluene (30 mL) was stirred at 75 °C for 12 h. The reaction mixture was precipitated using a methanol/chloroform mixture (5/1, *V*/*V*). The resulting precipitate was collected and dried under vacuum at 80 °C to afford compound **1a** as a pale yellow solid (400 mg, 58% yield). ^{1}H-NMR (400 MHz, 10% TFA in $CDCl_3$, Fig. S31 in ESI, δ, ppm): 7.67 (s, 4H), 7.52 (d, *J*=44.9 Hz, 8H), 7.44 (s, 4H), 6.92 (s, 4H), 5.30 (s, 2H), 4.04 (t, *J*=32.2, 6.6 Hz, 13H), 3.78 (s, 4H), 1.72 (m, 25H), 1.26 (s, 77H), 0.87 (t, *J*=6.6 Hz, 22H), 0.40 (d, *J*=6.1 Hz, 16H), 0.23–0.18 (m, 13H), 0.08 (s, 369H).

Compound **1b** was synthesized analogously as a pale yellow solid (60% yield). ^{1}H-NMR (400 MHz, 10% TFA in $CDCl_3$, Fig. S32 in ESI, δ, ppm): 7.66 (s, 4H), 7.57 (s, 8H), 7.46 (s, 4H), 6.92 (s, 4H), 5.33 (s, 2H), 4.04 (m, 14H), 3.76 (s, 4H), 1.89–1.56 (m, 28H), 1.26 (s, 78H), 0.87 (t, *J*=6.5 Hz, 23H), 0.08 (s, 391H).

Crystal Structure Determination

Single crystals of **4** suitable for X-ray structural analysis, were obtained by diffusing acetonitrile into DMF solutions at room temperature. X-ray diffraction data were collected on an XtaLAB Synergy X-ray diffractometer using Cu Kα radiation (λ=1.5418 Å). The structure was solved with the SHELXT structure solution program using Intrinsic Phasing and refined with the SHELXL refinement package using least-squares minimization. The X-ray crystallographic coordinates for compound **4** were deposited at the Cambridge Crystallographic Data Centre (CCDC) under the deposition number CCDC 2525723. These data can be obtained free of charge from The Cambridge Crystallographic Data Centre at www.ccdc.cam.ac. The crystal data and processing parameters for **4** are summarized in Table S1 (in ESI).

RESULTS AND DISCUSSION

Synthesis of Squaramide-based Building Blocks

To implement a squaramide-directed cooperative assembly strategy, we first constructed compound **2** as the minimal hydrogen-bonding building block, followed by telechelic macromolecules **1a**/**1b** in which the assembling motifs were covalently tethered to the PDMS spacers (Scheme 1c). This modular design enables a direct comparison between discrete 1D nanofibers and their covalently integrated hierarchical polymer networks.

Compound **2** was obtained *via* nucleophilic substitution of mono-substituted squaramide precursor **7** with octylamine (Scheme S2 in ESI). The successful conversion was confirmed by ^{1}H-NMR spectroscopy, as indicated by the disappearance of the resonance at 4.9 ppm corresponding to the methylene protons adjacent to the oxygen atom of **7**, together with the emergence of a new signal at 3.8 ppm assigned to methylene protons adjacent to the squaramide unit (Figs. S1 and S25 in ESI). Furthermore, telechelic PDMS macromolecules **1a** ($M_n \approx$ 5 kg/mol) and **1b** ($M_n \approx$ 10 kg/mol) were synthesized by coupling. **7** with aminopropyl-terminated PDMS (Scheme S4 in ESI). The telechelic architecture was verified by ^{1}H-NMR spectroscopy (Figs. S1, S31 and S32 in ESI), which again showed the complete disappearance of the 4.9 ppm signal and the appearance of the diagnostic 3.8 ppm resonance. This structural design provides a controlled platform for evaluating how cooperative 1D assemblies translate into hierarchical network formation.

Self-assembly of Compound 2 into Cooperative 1D Nanofibers

The formation of well-defined 1D nanofibers is a prerequisite for translating molecular recognition into a hierarchical network formation. To validate the cooperative assembly capability of the squaramide–amide motif, we first investigated the solution-phase behavior of the model compound **2**. In dilute chloroform (c=20 μmol·L^{-1}, 298 K), compound **2** exhibited a broad absorption band centered at 332 nm (Fig. 1a), which is characteristic of its molecularly dissolved state.[42,43] When the solvent was changed to toluene, the absorption signals of **2** exhibited a clear blue shift, with the maximum π-π^* absorption signal shifting to 303 nm (Fig. 1a). Meanwhile, supramolecular chirality emerged in toluene: a strong bisignated Cotton effect appeared for **2**, with a positive maximum at 338 nm (g=0.007) and a negative maximum at 298 nm (g=–0.003, Fig. 1b), in stark contrast to the absence of Cotton effects in chloroform (Fig. 1b). No LD signal was observed for the CD-active sample (Fig. S2 in ESI), suggesting that no CD artifacts were caused by macroscopic alignment. Hence, self-assembly occurred in **2** in toluene, accompanied by chirality transfer from the stereogenic (1*S*)-phenylethyl units to the squaramide motif.

Temperature-dependent UV-Vis spectroscopy in toluene was performed to elucidate the self-assembly mechanism of **2**. A non-sigmoidal melting transition was acquired over 293–363 K, consistent with a cooperative nucleation-elongation mechanism (Fig. 1c and Fig. S3 in ESI). Fitting the data with a mass-balance model for the 1D nanofiber assembly afforded a critical elongation temperature (T_e) of 337.4 K and a cooperativity factor (σ) of 0.00002. A low σ value reflects the pronounced cooperativity of the self-assembly process. The number-averaged degree of polymerization ($<N_n>$) was calculated as 870 at 298 K (Fig. S4 in ESI). Collectively, these results support the formation of long-range-ordered 1D assemblies in toluene. This conclusion was further corroborated by atomic force microscopy (AFM), which revealed nanofibers extending several micrometers in length (Fig. 1d).

Structural Origin of Orthogonal Cooperative Assembly

To gain molecular-level insights into the packing mode underlying the cooperative 1D assembly of **2**, we attempted to obtain single crystals suitable for X-ray diffraction. Although the crystallization of **2** was unsuccessful, mono-substituted analog **4** (Fig. 2a) afforded high-quality single crystals, allowing structural analysis of the fundamental hydrogen-bonding motif (Fig. 2b). Compound **4** crystallized in the centrosymmetric space group $P2_1/n$ (Z=4), revealing two distinct and spatially separated hydrogen-bonding arrays. The amide groups form intermolecular N—H···O hydrogen bonds with alternating distances of 2.14 and 2.06 Å, while the squaramide units display a uniform N—H···O distance of 2.07 Å, with an orthogonal recognition mode between these two hydrogen-bonding motifs.

To clarify how disubstituted squaramides influence intermolecular interactions, DFT calculations were performed on energy-minimized dimers of compound **5** (Fig. 2a), a disubstituted analog of compound **2** devoid of alkyl side chains. The orthogonal assembly mode (–0.071294 *Hartree*) was signifi-

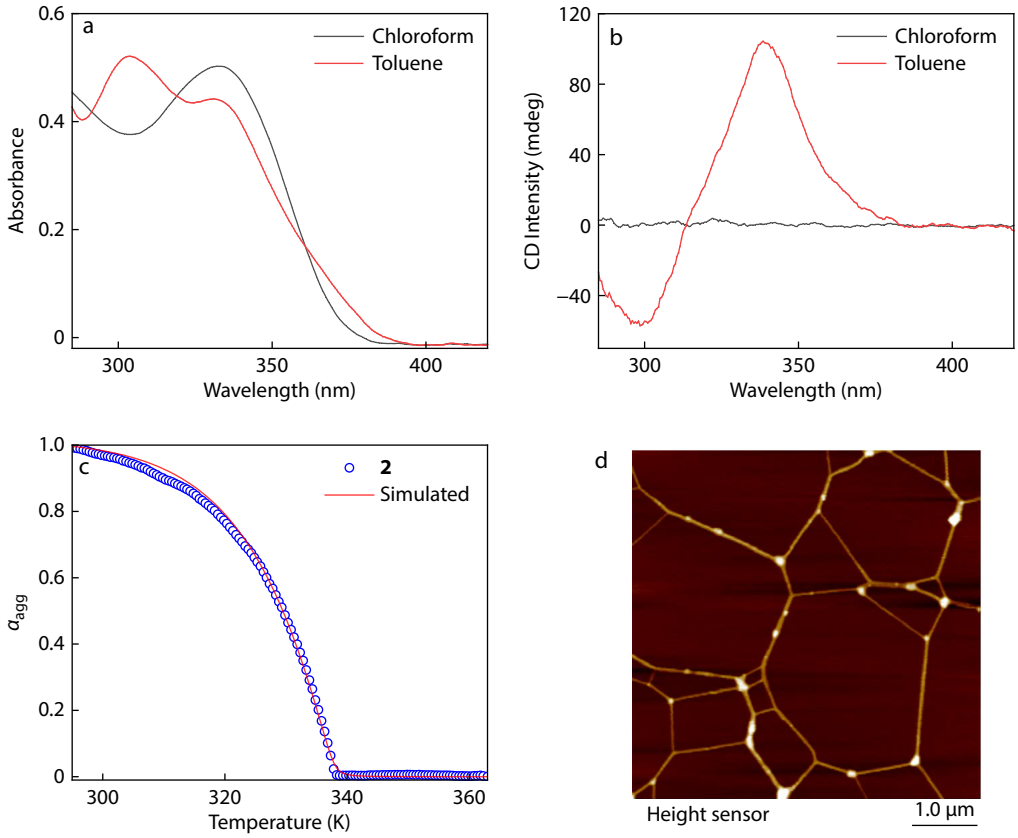

Fig. 1 (a) UV–Vis spectra (c=20 μmol·L^{-1}, 298 K) of **2** in chloroform (black line) and toluene (red line); (b) CD spectra (c=20 μmol·L^{-1}, 298 K) of **2** in chloroform (black line) and toluene (red line); (c) The normalized cooling curve (α_{agg}: degree of aggregation) of **2** (c=20 μmol·L^{-1} in toluene), acquired by monitoring the UV-Vis intensity changes at 306 nm; (d) AFM height image of **2**. [prepared by spin coating the sample in toluene (c=20 μmol·L^{-1}) into mica].

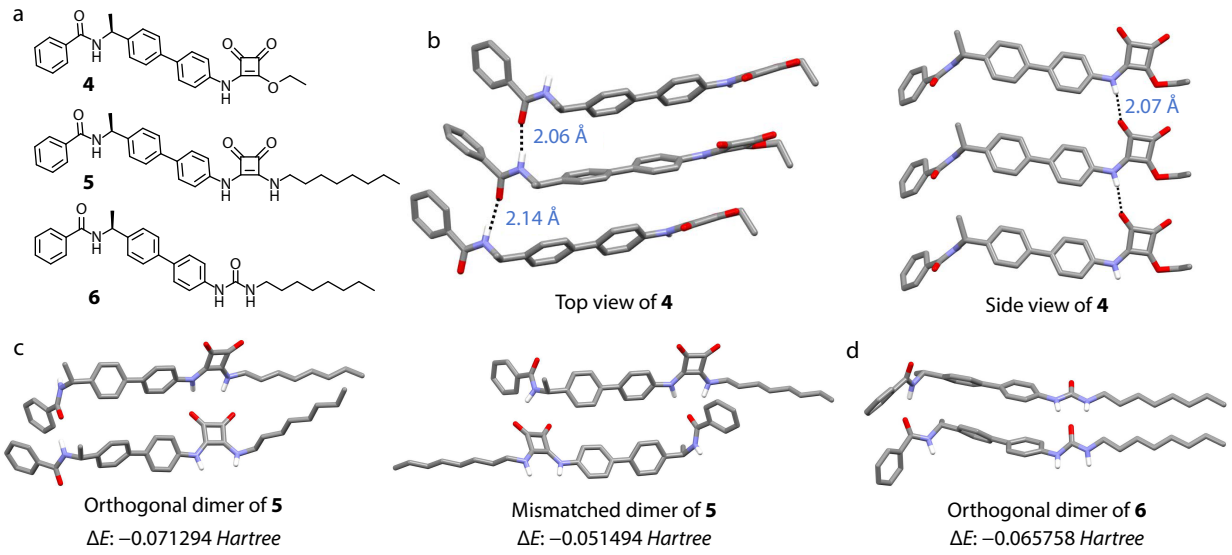

Fig. 2 (a) Chemical structures of the model compounds **4**–**6**; (b) Single-crystal structure of compound **4** (CCDC: 2525723); (c, d) Optimized dimeric structures of (c) **5** and (d) **6** obtained from DFT calculations; relative energies were calculated at the same level of theory.

cantly more stable than the mismatched configuration (–0.051494 *Hartree*), establishing a clear energetic hierarchy between the two packing arrangements (Fig. 2c). This energetic preference aligns with the orthogonal packing geometry observed in the single-crystal structure of mono-substituted analog **4**.

Notably, the disubstituted squaramide units in **5** formed dual hydrogen bonds, which substantially enhanced the intermolecular stabilization relative to mono-substituted systems. This is supported by solution-phase self-assembly stud-

ies of compound **7**, a mono-substituted analog of **4** differing only by the incorporation of solubilizing alkyl chains. No CD signal was detected for **7** in toluene (Fig. S5a in ESI), in stark contrast to the pronounced CD intensity observed for compound **2** (Fig. 1b), the disubstituted analog of **5**, whereas a distinct CD response for **7** only emerged in the less polar solvent methylcyclohexane (MCH) (Fig. S5b in ESI). AFM measurements corroborated these findings, revealing discrete nanoparticles for compound **7** and well-defined nanofibers for compound **2** (Fig. S6 in ESI). Collectively, these results demonstrate that the disubstituted squaramide unit not only favors the orthogonal assembly mode but also strengthens intermolecular binding, thereby promoting directional and cooperative supramolecular assembly into ordered 1D nanostructures.[44,45]

Energetic and Thermodynamic Advantages of Squaramide over Urea

To further elucidate the specific role of the squaramide motif in stabilizing the cooperative 1D assembly, we compared compound **2** with the structurally analogous urea derivative **3**. Because the absorption of the urea moiety overlaps with that of toluene,[46] spectroscopic monitoring of the assembly of **3** in toluene was impeded; therefore, MCH was selected as the assembly solvent. Nevertheless, the pronounced Tyndall effect observed in toluene (Fig. S7a in ESI), combined with the AFM images revealing the presence of nanoparticles (Fig. S7b in ESI), provides clear evidence that compound **3** indeed undergoes assembly in this solvent. To quantitatively compare the assembly propensities of **2** and **3**, we conducted solvent-dependent CD measurements by progressively increasing the fraction of polar chloroform in MCH (Figs. 3a, 3b and Figs. S8, S9 in ESI). When the solvent composition was changed from pure MCH to a mixture containing 10% chloroform, the CD intensity of **2** at 300 nm decreased by 2%, whereas that of **3** decreased by 29%. Upon further increasing the chloroform content to 25%, the CD signal of **3** disappeared completely, whereas **2** retained 91% of its original intensity. Collectively, these results demonstrate that the squaramide motif confers enhanced tolerance of supramolecular assemblies to solvent polarity.

To further substantiate the superior assembly capability of the squaramide motif, we conducted temperature-dependent CD measurements of MCH. CD spectra were recorded at 10 K intervals from 293 K to 333 K to monitor the evolution of the signals upon heating. As the temperature increased from 293 K to 313 K, the CD intensity of **3** at 280 nm decreased by 30%; a further 10 K increase led to an 84% reduction, and at 333 K, above the critical nucleation temperature, the CD signal vanished completely (Figs. 3c, 3d, and Fig. S10 in ESI). In sharp contrast, the CD signal of **2** remained essentially unchanged over the entire temperature range (Figs. 3c, 3d and Fig. S10 in ESI). demonstrating its resistance to thermally induced disassembly in MCH, and revealed a markedly higher thermal stability than that of **3**. Taken together, CD measurements under varying temperatures and solvent conditions consistently indicated the substantially enhanced stability of squaramide-based assemblies. This stability difference was

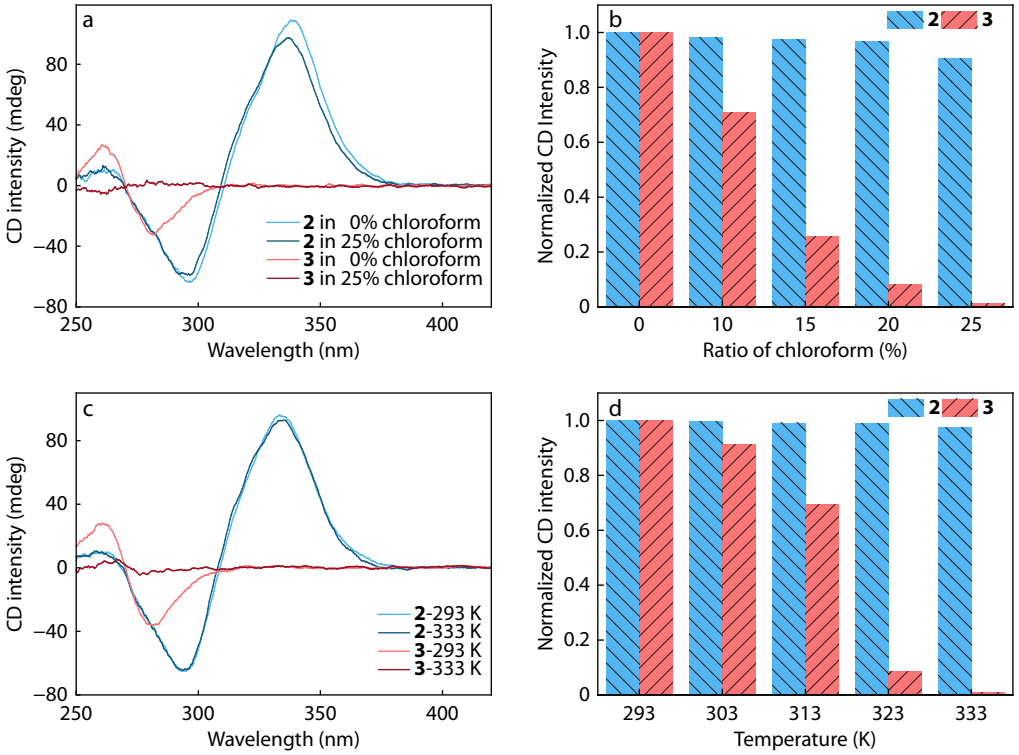

Fig. 3 (a) Solvent-dependent CD spectra of **2** (blue) and **3** (red) in MCH and MCH/chloroform (75/25, *V*/*V*) mixtures at 298 K (*c*=20 μmol·L^{-1}); (b) Normalized CD intensities of **2** (blue, monitored at 300 nm) and **3** (red, monitored at 280 nm) as a function of chloroform volume fraction (0% to 25% *V*/*V*) at 298 K (*c*=20 μmol·L^{-1}). (c) Temperature-dependent CD spectra of **2** (blue) and **3** (red) in MCH recorded at 293 K and 333 K (*c*=20 μmol·L^{-1}). (d) Normalized CD intensities of **2** (blue, monitored at 300 nm) and **3** (red, monitored at 280 nm) as a function of temperature from 293 K to 333 K in MCH (*c*=20 μmol·L^{-1}).

https://doi.org/10.1007/s10118-026-3700-z

further reflected in their macroscopic gelation behavior; compound **2** formed a stable gel in chloroform, whereas compound **3** did not (Fig. S11 in ESI). Consistent with this observation, AFM imaging revealed nanoparticle formation in compound **3**, while compound **2** exhibited well-defined nanofibrous assemblies (Fig. S12 in ESI). The formation of the long-range ordered fibrous architectures in **2** provides a structural basis for robust hierarchical fibril networks.

Based on the experimental observations, the intermolecular interactions in squaramide-based compound **2** were evidently stronger than those in urea analog **3**. This conclusion is further corroborated by DFT calculations: energy-minimized dimer models reveal that the dimer of **5** (Fig. 2a) exhibits a more negative binding energy than its urea counterpart **6** (–0.071294 versus –0.065758 *Hartree*, Figs. 2(c), 2(d) and Fig. S13 in ESI). These findings highlight the clear advantage of incorporating squaramide motifs in the construction of 1D nanofibers. This stems from the unique molecular features of squaramide: four-membered cyclobutenedione is aromatic, and hydrogen bond formation further enhances its cyclic aromaticity.[47,48] The cooperative interplay between aromaticity and hydrogen bonding endows squaramide-based systems with superior thermodynamic stability and sustained 1D supramolecular organization.

Translation of Cooperative 1D Assembly into Covalently Integrated Hierarchical Polymer Networks

Having established that squaramide-directed interactions promote highly cooperative 1D nanofibers, we investigated whether such assemblies could be translated into covalently integrated hierarchical polymer networks through telechelic architecture design. Telechelic macromolecule **1a**, in which the squaramide–amide recognition units are tethered to PDMS spacers (M_n≈5 kg/mol), was first examined in solution. In a toluene/tetrachloroethane mixture (2/1, *V*/*V*; c=1.0×10^{-5} mol·L^{-1}) at 358 K, the π-π* transition of the squaramide moiety appears at 336 nm, corresponding to a molecularly dissolved state (Fig. S14a in ESI). Upon cooling to 298 K, the absorption maximum shifted to 300 nm, accompanied by the emergence of a bisignate Cotton effect (Fig. S14b in ESI), indicative of self-assembly with the emergent supramolecular chirality signal. These results confirmed that covalent tethering to PDMS does not disrupt the intrinsic cooperative 1D assembly of the squaramide motif.

We then examined whether covalent integration influenced assembly stability. To enable a meaningful comparison of solution-phase stability, the concentrations of squaramide motifs in **1a** and **2** were carefully matched in toluene, and temperature-dependent CD spectroscopy was employed to monitor the changes in CD intensity upon heating. The results indicated that **1a** did not reach a fully monomeric state upon heating; even at 343 K, the CD intensity decreased by only 33% relative to that at 293 K (Figs. 4a, 4b and Fig. S15a in ESI). In contrast, the CD signal of **2** disappeared completely at 343 K, indicating a fully monomeric state under identical conditions. (Figs. 4a, 4b and Fig. S15b in

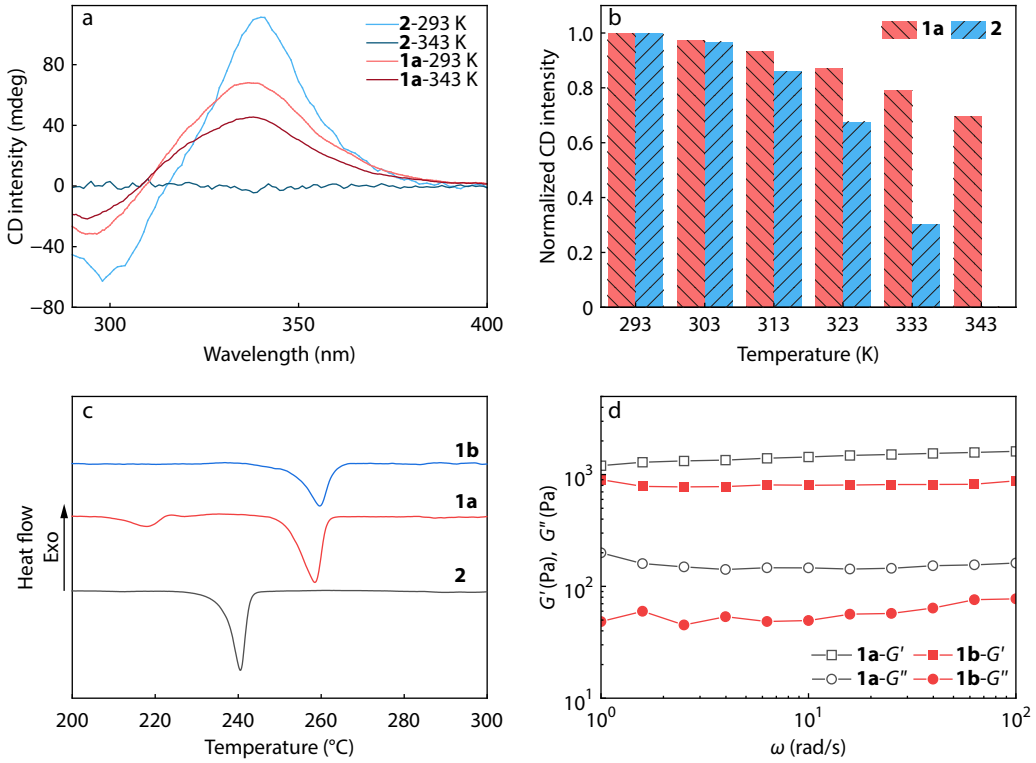

Fig. 4 (a) Temperature-dependent CD spectra of **1a** (red) and **2** (blue) in a toluene/tetrachloroethane mixture (2/1, *V*/*V*, c=10 μmol·L^{-1}) at 293 and 343 K. (b) Normalized CD intensity of **1a** (red, monitored at 335 nm) and **2** (blue, monitored at 340 nm) as a function of temperature from 293 K to 343 K in a toluene/tetrachloroethane mixture (2/1, *V*/*V*, c=10 μmol·L^{-1}). (c) DSC curves of **2** (black), **1a** (red), and **1b** (blue) acquired from the first heating process. (d) Frequency-dependent oscillatory rheology of **1a** (black) and **1b** (red) at 40 g/L in chloroform at 20 °C, showing the storage modulus (G') and loss modulus (G'').

https://doi.org/10.1007/s10118-026-3700-z

ESI). These findings clearly demonstrate that the 3D crosslinked networks exhibit significantly higher stability than the 1D nanofibers in solution.

Bulk-phase analysis further elucidated the stability implications of integrating discrete 1D nanofibers into a hierarchical fibrillar network. Differential scanning calorimetry (DSC) was used to quantitatively compare the thermal behavior in the bulk state. Compound **1a** exhibited a higher melting temperature (258.5 °C) than **2** (240.4 °C, Fig. 4c), indicating a greater energetic penalty for disrupting the assembled architecture in the telechelic system. Collectively, these findings demonstrate that telechelic macromolecular design enables the structural integration of cooperatively assembled nanofibers into a covalently interconnected network, thereby enhancing macroscopic stability.

Hydrogen-bond Density Governs Network Architecture and Mechanical Response

To examine how hydrogen-bond density influences hierarchical network formation and macroscopic mechanics, telechelic macromolecule **1b** was synthesized with a longer PDMS spacer (M_n≈10 kg/mol), thereby reducing the effective density of the squaramide recognition units while preserving identical terminal motifs. Gelation experiments provide an initial qualitative assessment of the gel-forming ability. Increasing the PDMS spacer length increased the critical gelation concentration (CGC) from 10 g/L for **1a** to 30 g/L for **1b** (Fig. S16 in ESI), indicating that a higher concentration is required to establish a self-supporting network. Oscillatory rheological measurements at 40 g/L further elucidated the viscoelastic response arising from this structural variation (Fig. 4d). Both systems exhibit a frequency-independent storage modulus (G') exceeding the loss modulus (G'') over 1–100 rad·s^{-1}, which is consistent with the formation of elastic hierarchical polymer networks. Notably, **1a** displayed substantially higher moduli than **1b**, which is consistent with the greater density of squaramide-mediated crosslinks.

To understand the molecular basis of the mechanical differences between **1a** and **1b**, we examined the effect of hydrogen-bond density on the assembly behavior. Variable-temperature CD measurements show a decrease in the critical elongation temperature (T_e) from 343.7 K for **1a** to 333.5 K for **1b** (Fig. S17 in ESI), indicating reduced stability of the hierarchical fibrillar network at lower hydrogen-bond densities. AFM imaging revealed fibrous nanostructures for both macromolecules, with **1a** forming longer and more continuous fibers than **1b** (Fig. S18 in ESI), which is consistent with its superior mechanical performance. The fibrous morphology reflects the 1D hydrogen-bonded assembly of the squaramide units embedded within the PDMS matrix, generating a microphase-separated architecture of hard squaramide domains and soft PDMS segments that underlie the mechanical integrity of the hierarchical network.[48,49] Taken together, these results demonstrate that increasing the hydrogen-bond density from **1b** to **1a** strengthens the cooperative 1D assembly, thereby improving the mechanical robustness of the hierarchical polymer network.

CONCLUSIONS

In summary, we demonstrated that heterogeneous squaramide–amide hydrogen-bonding motifs promote cooperative, orthogonal 1D assembly into long-range nanofibers. Comparative studies with a urea analog confirmed the critical role of the squaramide unit in enhancing intermolecular binding and assembly stability. By covalently incorporating these assembling motifs into telechelic PDMS, discrete nanofibers were integrated into a microphase-separated, covalently interconnected hierarchical network. This structural integration leads to enhanced thermal stability and mechanical rigidity relative to those of small-molecule systems. Variation in the assembling segment content modulates hydrogen-bond density and supramolecular organization, establishing a direct structure-property relationship between cooperative 1D assembly and macroscopic mechanical performance. These results illustrate how squaramide-directed cooperative assembly can be translated into hierarchical polymer networks through covalent macromolecular integration, providing a molecular-level strategy for designing polymer networks with controllable architectures and mechanics.

Conflict of Interests

The authors declare no interest conflict.

Electronic Supplementary Information

Electronic supplementary information (ESI) is available free of charge in the online version of this article at http://doi.org/10.1007/s10118-026-3700-z.

Data Availability Statement

The data supporting the findings of this study are available from the corresponding author upon reasonable request.

ACKNOWLEDGMENTS

This study was financially supported by the National Natural Science Foundation of China (Nos. 22371272 and 92356302) and the International Partnership Program of the Chinese Academy of Sciences (No. 123GJHZ2022064MI). We are grateful for the technical support provided by the High Performance Computing Center of the University of Science and Technology of China for the DFT and TD-DFT computations.

REFERENCES

1 Chen, T.; Xu, J.; Wang, C.; Zhang, X.; Pei, X.; Wang, T.; Wang, Q. Shape-memory polyurethanes for polar wearables with ultrasensitive multi-monitoring. *Nat. Commun.* **2025**, *16*, 11329.
2 Li, Y.; Sun, J. Reversibly cross-linked polymers: a new method for high-performance and sustainable polymer materials. *Acc. Chem. Res.* **2026**, *59*, 298–310.
3 Adane, A. M.; Park, S.Y. Photonic interpenetrating polymer network fibers comprising intertwined solid-state cholesteric liquid crystal and polyelectrolyte networks for sensor applications. *ACS Appl. Mater. Interfaces* **2024**, *16*, 16830–16843.
4 Zhang, Q.; Xu, Z. Y.; Liu, W. G. Hydrogen-bonding crosslinked supramolecular polymer materials: from design evolution of

Graphical Abstract

Squaramide-directed Cooperative One-dimensional Assembly in Telechelic polydimethylsiloxane for Hierarchical Network Formation

Yu-Hong Zhang, Jian-Fei Ma, Hao-Bo Wei, Jie Wang, and Feng Wang

University of Science and Technology of China; Jilin University of Chemical Technology

A squaramide-directed cooperative assembly strategy was developed to construct hierarchical polymer networks by integrating 1D supramolecular nanofibers into covalent architectures. This approach effectively reconciles the trade-off between covalent robustness and supramolecular reversibility, leading to a significantly enhanced thermal stability and mechanical performance.

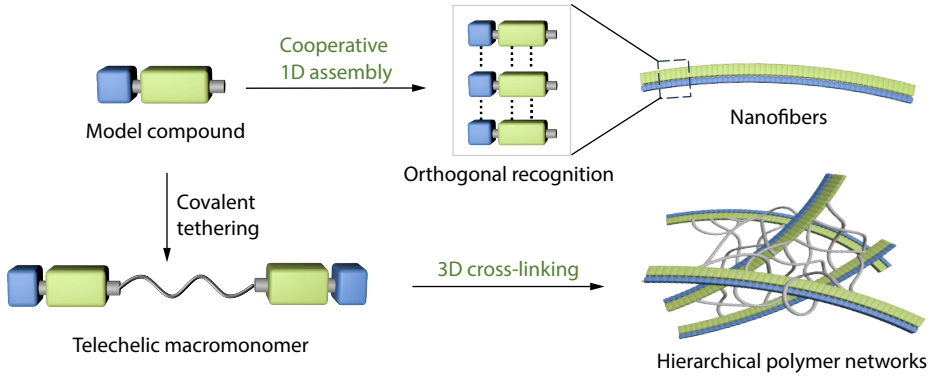

Chinese J. Polym. Sci., 2026 *https://doi.org/10.1007/s10118-026-3700-z*

side-chain hydrogen-bonding to applications. *Chinese J. Polym. Sci.* **2024**, *42*, 1619–1641.
5 Ollier, R. C.; Webber, M. J. Mechanoresponsive hydrogels emerging from dynamic and non-covalent interactions. *Adv. Mater.* **2025**, *37*, 2507397.
6 Zhao, J.; Zhang, Z.; Wang, C.; Yan, X. Synergistic dual dynamic bonds in covalent adaptable networks. *CCS Chem.* **2024**, *6*, 41–56.
7 Gao, W.; Chen, Z.; Shao, M.; Huang, H.; Hong, J.; Zhang, Q.; Fang, Y.; Shi, W.; Dong, J.; Guo, Y.; Chen, J.; Liu, Y. Leveraging conformational locking to synthesize acylhydrazone-linked covalent organic frameworks with aggregation-induced-emission nodes. *CCS Chem.* **2026**, *8*, 989–1000.
8 Shi, C.Y.; Zhang, Q.; Wang, B.S.; He, D.D.; Tian, H.; Qu, D.H. Highly ordered supramolecular assembled networks tailored by bioinspired h-bonding confinement for recyclable ion-transport materials. *CCS Chem.* **2023**, *5*, 1422–1432.
9 Cao, Z.; Yang, Z.; Wang, W.; Li, P.; Sun, Y.; An, W.; Liu, G.; Zheng, X.; Niu, C.; Rao, S.; Zhang, W. Dynamic supramolecular network crosslinked by hydrogen bonds and pillar[5]arene-based host–guest interaction. *Chin. Chemical Lett.* **2026**, *37*, 112104.
10 Wang, Y.H.; Deng, J.X.; Zhao, J.; Ding, Y.; Yang, L.; Zhang, Z.M.; Yan, X.Z. Bolstering the mechanical robustness of supramolecular polymer network by mechanical bond. *Chinese J. Polym. Sci.* **2024**, *42*, 1536–1544.
11 Xue, Y.; Huang, Y.; Chen, S.; Ma, J.; Xiao, S.; Wang, F. Energy landscape modulation enables helicity overriding in supramolecular copolymers. *Nat. Synth.* **2026**, *5*, 84–94.
12 Zhang, Y.; Xue, Y.; Gao, L.; Liao, R.; Wang, F.; Wang, F. Merging non-covalent and covalent crosslinking: En route to single chain nanoparticles. *Chin. Chem. Lett.* **2024**, *35*, 109217.
13 Anton, C.; Lautenschläger, F.; Hawkins, R. J. Modeling cytoskeletal and cell dynamics. *Curr. Opin. Cell Biol.* **2025**, *97*, 102584.
14 Wang, S.; Zhang, L.; Wang, Z.; Song, Z.; Liu, H.; Tian, Z.; Xu, X. Humidity-adaptive, mechanically robust, and recyclable bioplastic films amplified by nanoconfined assembly. *Aggregate* **2024**, *5*, e643.
15 Zhou, X.; Li, Z. Advances and biomedical applications of polypeptide hydrogels derived from α-amino acid N-carboxyanhydride (NCA) polymerizations. *Adv. Healthc. Mater.* **2018**, *7*, 1800020.
16 ter Huurne, G. M.; Palmans, A. R.; Meijer, E. Supramolecular single-chain polymeric nanoparticles. *CCS Chem.* **2019**, *1*, 64–82.
17 Zhu, X.; Ma, J.; Zhang, D.; Fang, Z.; Zhang, J.; Wang, M.; Zhang, M.; Tang, B.-Z.; Li, Y. Mechanically active adhesive and NIR-II-activated zwitterionic hydrogel for infected maxillofacial wound repair and abscess elimination. *Aggregate* **2026**, *7*, e70309.
18 Zhang, L.; Zhou, X.; Xiong, X.; Cui, J. Polymer fibers based on dynamic covalent chemistry. *Chinese J. Polym. Sci.* **2025**, *43*, 245–260.
19 Goor, O. J.; Hendrikse, S. I.; Dankers, P. Y.; Meijer, E. From supramolecular polymers to multi-component biomaterials. *Chem. Soc. Rev.* **2017**, *46*, 6621–6637.
20 Li, Z.; Lin, Z. Recent advances in polysaccharide-based hydrogels for synthesis and applications. *Aggregate* **2021**, *2*, e21.
21 Storm, C.; Pastore, J. J.; MacKintosh, F. C.; Lubensky, T. C.; Janmey, P. A. Nonlinear elasticity in biological gels. *Nature* **2005**, *435*, 191–194.

22 Hafeez, S.; Decarli, M. C.; Aldana, A.; Ebrahimi, M.; Ruiter, F. A. A.; Duimel, H.; van Blitterswijk, C.; Pitet, L. M.; Moroni, L.; Baker, M. B. *In situ* covalent reinforcement of a benzene-1, 3, 5-tricarboxamide supramolecular polymer enables biomimetic, tough, and fibrous hydrogels and bioinks. *Adv. Mater. Deerfield Beach Fla* **2023**, *35*, e2301242.

23 Sathyan, A.; Deng, L.; Loman, T.; Palmans, A. R. Bioorthogonal catalysis in complex media: consequences of using polymeric scaffold materials on catalyst stability and activity. *Catal. Today* **2023**, *418*, 114116.

24 Liu, X.; Sun, J. Polymeric materials reinforced by noncovalent aggregates of polymer chains. *Aggregate* **2021**, *2*, e109.

25 Lu, F.; Chen, Y.; Fu, B.; Chen, S.; Wang, L. Multistimuli responsive supramolecular polymer networks *via* host-guest complexation of pillararene-containing polymers and sulfonium salts. *Chin. Chemical Lett* **2022**, *33*, 5111−5115.

26 Dai, W. T.; Xie, Z. H.; Ke, Y. B.; You, Y.; Rong, M. Z.; Zhang, M. Q. Topological confinement in reversibly interlocked polymer networks. *Chinese J. Polym. Sci.* **2024**, *42*, 133−140.

27 Jin, B.; Li, Q.; Hu, L.; Liu, Q.; Chen, Y.; Luo, Y.; Chi, S.; Li, X. In situ nucleation-growth strategy for controllable heterogeneous supramolecular polymerization of liquid crystalline block copolymers and their hierarchical assembly. *Angew. Chim.* **2023**, *135*, e202219067.

28 Ma, J.; Jiang, S.; Tan, X.; Tian, Y.; Dong, S.; Wang, F. Tough supramolecular glasses enabled by frustrated non-covalent complexation. *Angew. Chim.* **2025**, *137*, e202519907.

29 Duong, T. K. N.; Truong, T. T.; Phan, T. N. L.; Nguyen, T. X.; Doan, V. H. M.; Vo, T. T.; Choi, J.; Pal, U.; Dhar, P.; Lee, B.; Oh, J.; Mondal, S. Hydrogel-based smart materials for wound healing and sensing. *Aggregate* **2025**, *6*, e70047.

30 Li, Z.; Zhu, Y. L.; Niu, W.; Yang, X.; Jiang, Z.; Lu, Z. Y.; Liu, X.; Sun, J. Healable and recyclable elastomers with record-high mechanical robustness, unprecedented crack tolerance, and superhigh elastic restorability. *Adv. Mater.* **2021**, *33*, 2101498.

31 Guang, L. Y.; Zhou, Z. F.; Zhang, Y. F.; Gao, L.W.; Wang, F.; Liao, R. Cooperative supramolecular polymerization of propeller-shaped triphenylamine cyanostilbenes for explosive detection. *Chinese J. Polym. Sci.* **2023**, *41*, 585−592.

32 Xiao, T.; Zhou, L.; Sun, X.Q.; Huang, F.; Lin, C.; Wang, L. Supramolecular polymers fabricated by orthogonal self-assembly based on multiple hydrogen bonding and macrocyclic host–guest interactions. *Chin. Chem. Lett.* **2020**, *31*, 1−9.

33 Zhao, Y.K.; Gao, Z.Z.; Wang, H.; Zhang, D.W.; Li, Z.T. Self-assembly of supramolecular polymers in water from tetracationic and tetraanionic monomers in water through cooperative electrostatic attraction and aromatic stacking. *Chin. Chemical Lett.* **2019**, *30*, 127−130.

34 Hafeez, S.; Aldana, A. A.; Duimel, H.; Ruiter, F. A.; Decarli, M. C.; Lapointe, V.; van Blitterswijk, C.; Moroni, L.; Baker, M. B. Molecular tuning of a benzene-1,3,5-tricarboxamide supramolecular fibrous hydrogel enables control over viscoelasticity and creates tunable ECM-mimetic hydrogels and bioinks. *Adv. Mater.* **2023**, *35*, 2207053.

35 Li, Y.; Wang, Y.; Wang, S.; Ye, Z.; Bian, C.; Xing, X.; Hong, T.; Jing, X. Highly tunable and robust dynamic polymer networks *via* conjugated–hindered urea bonds. *Macromolecules* **2022**, *55*, 9091−9102.

36 Deng, Y.; Zhang, Q.; Qu, D.H. Emerging hydrogen-bond design for high-performance dynamic polymeric materials. *ACS Mater. Lett.* **2023**, *5*, 480−490.

37 Wei, P.; Yan, X.; Huang, F. Supramolecular polymers constructed by orthogonal self-assembly based on host–guest and metal–ligand interactions. *Chem. Soc. Rev.* **2015**, *44*, 815−832.

38 Wu, J.; Cai, L. H.; Weitz, D. A. Tough self-healing elastomers by molecular enforced integration of covalent and reversible networks. *Adv. Mater.* **2017**, *29*, 1702616.

39 Xue, Y.; Jiang, S.; Zhong, H.; Chen, Z.; Wang, F. Photo-induced polymer cyclization *via* supramolecular confinement of cyanostilbenes. *Angew. Chim. Int. Ed.* **2022**, *61*, e202110766.

40 Lv, T.; Wu, S.; Jin, Y.; Ma, J.; Jiang, S.; Xue, Y.; Wang, F. Enhancing the circularly polarized luminescence of self-assembled cyanostilbenes through extended π-conjugation. *Chin. J. Chem.* **2024**, *42*, 135−141.

41 Nishikawa, J.; Imase, T.; Koike, M.; Fukuda, K.; Tokita, M.; Watanabe, J.; Kawauchi, S. Internal rotations of aromatic polyamides: a density functional theory study. *J. Mol. Struct.* **2005**, *741*, 221−228.

42 Saez Talens, V.; Englebienne, P.; Trinh, T. T.; Noteborn, W. E.; Voets, I. K.; Kieltyka, R. E. Aromatic gain in a supramolecular polymer. *Angew. Chim. Int. Ed.* **2015**, *54*, 10502−10506.

43 Bujosa, S.; Rubert, L.; Rotger, C.; Soberats, B. Modulating self-assembly and polymorph transitions in bisdendronized squaramides. *Commun. Chem.* **2024**, *7*, 296.

44 Chen, J.; Yu, N.; Zhang, H.; Wei, Y.; He, Y.; Sha, Y.; Li, G.; Zhang, M.; Luo, Y.; Luo, Z. Strong and colorless transparent polyurethanes enabled by squaramide units: from flexibility to stiffness. *ACS Appl. Polym. Mater.* **2025**, *7*, 8300−8310.

45 Konar, D.; Stewart, K. A.; Moerschel, J.; Rynk, J. F.; Sumerlin, B. S. Polysquaramides. *ACS Macro Lett.* **2024**, *13*, 972−978.

46 Cao, H.; Li, B.; Jiang, X.; Zhu, X.; Kong, X. Z. Fluorescent linear polyurea based on toluene diisocyanate: Easy preparation, broad emission and potential applications. *ACS Appl. Polym. Mater.* **2020**, *399*, 125867.

47 Bujosa, S.; Castellanos, E.; Frontera, A.; Rotger, C.; Costa, A.; Soberats, B. Self-assembly of amphiphilic aryl-squaramides in water driven by dipolar π−π interactions . *Org. Biomol. Chem.* **2020**, *18*, 888−894.

48 Storer, R. I.; Aciro, C.; Jones, L. H. Squaramides: physical properties, synthesis and applications. *Chem. Soc. Rev.* **2011**, *40*, 2330−2346.

49 Tian, J.; Zhou, Z.; Miao, X.; Wang, S.; Ming, Y.; Nie, Y.; Ma, Y.; Li, Z. Supertough, resilient, and healable thermoplastic poly (urethane urea) elastomers by dense packing of hydrogen-bonding arrays. *Adv. Funct. Mater.* **2026**, *36*, e04882.